Siloxene: A potential layered silicon intercalation anode for Na, Li and K ion batteries

Laura Loaiza, Laure Monconduit, Vincent Seznec

HAL Id: hal-02089369

https://hal.umontpellier.fr/hal-02089369v1

Submitted on 22 Oct 2021

Siloxene: A potential layered silicon intercalation anode for Na, Li and K ion batteries

Laura C. Loaiza [a], Laure Monconduit [b,c,d], Vincent Seznec [a,c,d],*

[a] Laboratoire de Réactivité et Chimie des Solides (CNRS UMR 7314), Université de Picardie Jules Verne, 33 Rue Saint Leu, 80039 Amiens Cedex, France.

[b] Institut Charles Gerhardt -AIME (CNRS UMR 5253), Université de Montpellier CC 15-02, Pl. E. Bataillon, 34095 Montpellier Cedex 5, France.

[c] Réseau sur le Stockage Electrochimique de l'Energie (RS2E), CNRS FR3459, 33 Rue Saint Leu, 80039 Amiens, Cedex, France

[d] ALISTORE European Research Institute, Université de Picardie Jules Verne, 33 rue Saint Leu, 80039 Amiens Cedex, France

* Corresponding author.
E-mail: vincent.seznec@u-picardie.fr (Vincent Seznec)
        laura.loaiza@u-picardie.fr (Laura C. Loaiza)
        laure.monconduit@umontpellier.fr (Laure Monconduit)

Abstract

The alloying reaction between 14th group elements and alkali can be detrimental for Li, Na or K-ion batteries due to the large associated volume expansion that leads to a rapid capacity fading. In order to overcome this issue, their associated 2D phases are promising anodes that enable alkali intercalation without alloying reaction and volume expansion. In this study, the lamellar siloxene obtained from topotactic deintercalation of Ca from $CaSi_2$ delivered reversible capacities of 2300, 311 and 203 mAh/g for Li, Na and K, respectively, with good capacity retention and coulombic efficiency for Li and Na. The intercalation mechanism taking place upon cycling is highlighted on the basis of *ex situ* Raman characterization combined with IR spectroscopy, SEM and TEM. To the best of our knowledge, it is the first time that a lamellar Silicon based material shows such high stable capacity without volume expansion, representing a real breakthrough for the batteries field and particularly for NIB.

1

1. Introduction

Silicon is a crucial material for different technologies such as integrated circuits, photovoltaics, optoelectronics and most recently, batteries. It is one of the most promising anodes for lithium-ion (LIB) and sodium-ion (NIB) batteries due to its high theoretical capacity, 3590 mAh/g for $Li_{15}Si_4$[1] and 954 mAh/g for NaSi.[2] Nevertheless, its practical application is hindered by a series of obstacles. For lithium (Li), the access to such high lithiated phases causes extreme volume expansion (310%), resulting in a rapid capacity fade. For sodium (Na), the slow kinetics and the ionic radius restrict the sodiation of c-Si. In an attempt to address these problems, recent attention has been given to the two-dimensional 2D silicon structures, comprising calcium silicide ($CaSi_2$), polysilane (Si_6H_6) and siloxene ($Si_6O_3H_6$), due to their potential ability to buffer the electrode volume changes during cycling and their facile synthesis through soft-chemical methods. $CaSi_2$ has a Si- corrugated layered structure interconnected by Ca^{2+} ions. Upon reaction with concentrated HCl the Ca^{2+} is deintercalated while the integrity of the Si layers is preserved, producing the so-called Siloxene. [3,4] This topotactic reaction was first reported by Wöhler[5] and Kautsky[6] while Weiss *et al*[4] performed the structural characterization. Two structures were proposed; one with Si planes terminated by H or OH (Wöhler siloxene), and another one with Si_6 rings connected by oxygen bridges to form planes (Kautsky siloxene).

On the other hand, several theoretical studies have been done on siloxene nanosheets (Silicene). [7,8] The predictions show the possible intercalation of Li and Na with high theoretical capacities, low diffusion energy barrier (<0.6 eV for Li, 0.14eV for Na) and small volumetric expansion without any structural disintegration. [9–13] These promising theoretical studies have boosted the experimental research on this family of compounds for LIB. Recent reports include the use of different carbon coated silicon nanosheets and siloxenes as LIB anode with favorable cycling performance, attributed to the improved Li kinetics and limited volume changes due to the layered nature. [14–19] To our knowledge, no

2

experimental results on siloxene with NIB or potassium-ion batteries (KIB) have been reported.

In this work we have synthesized and characterized the siloxene, evaluated its electrochemical performance with Li, Na and K and formulated a possible electrochemical mechanism. The results show the versatility of siloxene as anode for LIB, NIB and KIB, opening a quest on a deeper understanding of this family of 2D materials.

2. Experimental Section

Synthesis: The $CaSi_2$ Zintl phase was synthesized by mixing stoichiometric amounts of Ca (99% ACROS Organics) and Si (325-Mesh, 99%, ACROS Organics) in an airtight 50 mL WC jar. The jar was rotated for 18 hours at 600 rpm, using a 10:2 ball:mass ratio, in a planetary ball mill (RETSCH PM 100). The resulting powders were loaded into stainless steel tubes sealed by arc welding under Ar and annealed at 800°C for 48 hours.

The siloxene was synthesized in air atmosphere, by dissolving ~300 mg of $CaSi_2$ in ~30 mL of HCl (35% VWR Chemicals) at -20°C for 8 hours. The greenish product was washed with distilled water and acetone, separated by centrifugation and vacuum dried for 1 hour.

All synthesis products were kept in an argon atmosphere to avoid further oxidation.

Characterization: The Powder XRD patterns were recorded in a Bruker D8 Advanced diffractometer with Cu radiation ($\lambda 1$ = 1.54056 Å, $\lambda 2$ = 1.54439 Å). The diffraction patterns were refined using the Fullprof software. Ex Situ Raman spectra were collected using a DXR 2 Raman Microscope. (Thermo-Fisher Scientific, 532-nm excitation). The Fourier transformed Infrared Spectra (Nicolet IS10, Themo-Fisher Scientific) were performed using KBr methods, an airtight cell with NaCl window was used for air sensitive samples. Particle morphology, size and microstructure were studied by scanning electron microscopy (SEM-environmental FEI Quanta 200 FEG microscope) and transmission electron microscopy (TEM-FEI Tecnai F20 S-TWIN).

Electrochemistry: Electrodes were prepared with a 1:1:1 mass ratio of active material, carbon super C_{45} and Carboxyl Methyl Celulose (CMC- DS = 0.9, Mw = 700 000 Aldrich), dissolved in distilled water with 0.4% of Triton X dispersant. The slurry was casted into copper foil using a doctor blade (50 µm thickness) and dried at ambient conditions for one day. 11.1 mm disks were cut and dried under vacuum at 70°C overnight. The siloxene electrodes were tested in half-cells against Li, Na and K using CR2032 coin cells, 1 M $LiPF_6$ ($NaPF_6$) in Ethylene Carbonate (EC)/Dimethyl Carbonate (DMC) [1:1] electrolyte with 1% Fluoro-ethylene carbonate (FEC) as additive, and a Whatman glass fiber separator (GF/ D, 675 µm). For K an electrolyte of 0.8M KFSI in EC/DEC (Diethyl Carbonate) showed the best stability. Alternative solvent mixtures were tested, EC/DEC, EC/PC (polycarbonate) and tetraglyme, the salt XPF_6 (X=Na, Li) concentration and ratio of FEC additive was kept constant. Galvanostatic cycling was performed at 25°C between 0 and 2 V versus Li/Li^+ (Na/Na^+) at the C/20 (C/n = 1Li (Na)/n h), using a VMP3 or MPG2 (Biologic) device.

3. Results and Discussion

3.1. Synthesis and Characterization of $CaSi_2$ and Siloxene

The $CaSi_2$ (space group R-3m) phase has two-dimensional corrugated layers of Si_6 rings separated by Ca atoms (**Figure 1a, S1, S2**), with several polymorphs that differ in their stacking sequences; among them, the 6R with an AABBCC sequence and the 3R with an ABC one.[4,20]. **Figure 1b** shows the diffraction pattern for the synthesized $CaSi_2$, the Le Bail refinement confirms that the polymorph is the 6R with a=3.8575(2) Å, c= 30.68(1) Å and V=395.42(3) $Å^3$ as cell parameters, in agreement with the literature (ICSD 248515).[21,22] Note that the peak intensity calculation presents some ambiguity due to a strong preferential stacking of the layers, as observed for other layered materials. [3,23] Lastly, the SEM picture (**Figure 1d**) confirms the lamellar character of $CaSi_2$.

Posteriorly, the siloxene ($Si_6H_3(OH)_3$) was prepared according to the Wöhler method, described by **equation 1**. The obtained product was a greenish-powder.
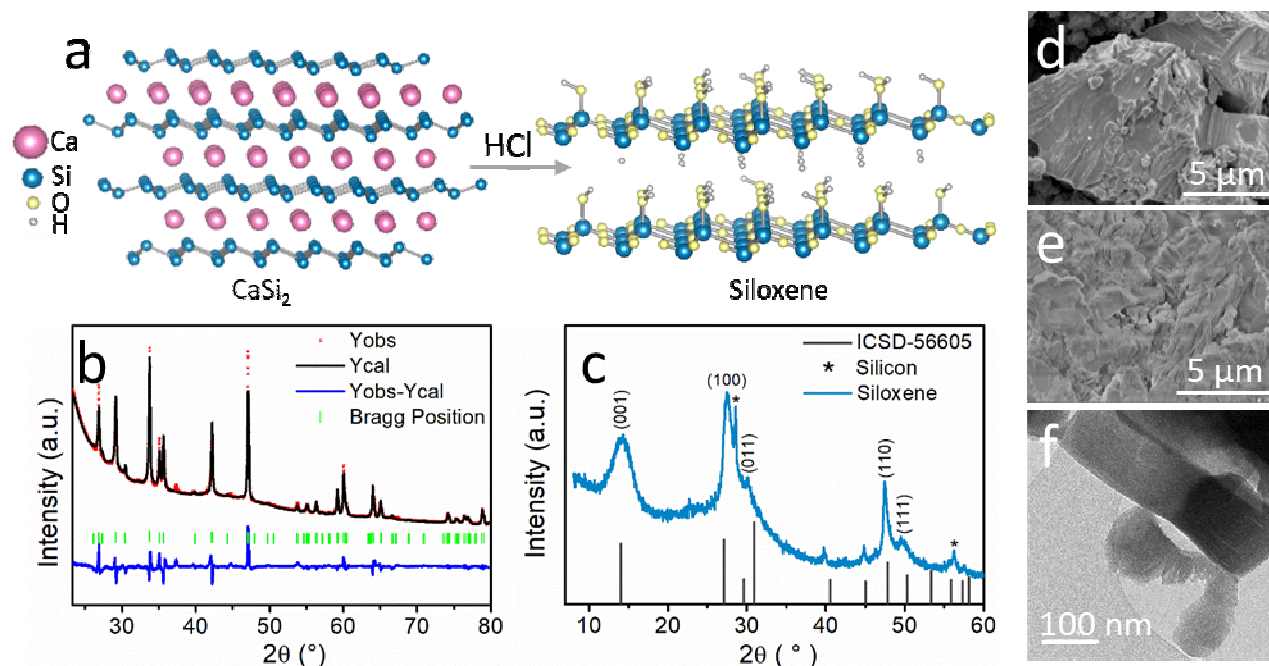
$$3CaSi_2 + 6HCl + 3H_2O \rightarrow Si_6H_3(OH)_3 + 3CaCl_2 + 3H_2 \text{ (g)} \tag{1}$$

Figure 1. **a)** Ilustration of the transformation of $CaSi_2$ into Siloxene upon reaction with HCl. **b)** Le Bail refinement for $CaSi_2$ XRD pattern. **c)** XRD pattern for siloxene. SEM images of **d)** $CaSi_2$ and **e)** siloxene. **f)** TEM image of siloxene

As observed in the SEM and TEM pictures (**Figure 1e,f**) the lamellar structure is preserved after Ca deinsertion. The XRD pattern (**Figure 1c**) shows broad peaks centered at 14, 27.7 and 47° accompanied with sharp reflections at 28 and 47°. The former ones are ascribed to the siloxene phase, the later ones to c-Si, originated during the synthesis through the formation of Si-Si bonds, as reported for other Zintl phases like KSi and NaSi.[3] The Le Bail refinement provided a cell parameter a=3.93(2) Å which is close to the value obtained for $CaSi_2$ (3.8575(2) Å), indicating the preservation of the corrugated layers. The c cell parameter, has slightly increased from 5.11(1) Å (c/6) in $CaSi_2$ to 6.092(5) Å in siloxene resulting in peak broadening and a larger interlayer separation, probably due to the incorporation of HCl, H_2O

or other functional groups.[3,4] Siloxene presents a more or less turbostratic stacking sequence, with some of the layers aligned with the center of a Si ring directly above the Si in the next layer and some others randomly stacked. Although as in $CaSi_2$ the 6R stacking sequence predominates. [3,24,25] Three different interpretations of the siloxene structure are reported in the literature; [3,4,26] corrugated silicon layers with three Si-Si bonds and alternating –H or –OH substituents as in Wöhler siloxene (a), two-dimensional Si sheets made of Si_6 rings linked by oxygen bridges, as in Kautsky Siloxene (b) and one-dimensional Si-Si chains interconnected by Si-O bonds (c) (**Figure S3**). The structure (a) has been reported to be metastable, with a gradual decomposition into Kautsky siloxene (b) through a hydrolysis process of Si-H to Si-OH and condensation to Si-O-Si, enhanced by light and UV irradiation.[4,27] Nonetheless, there is few experimental evidence for structures (b) and (c).[3,28] We believe that our siloxene is conformed to the Wöhler siloxene, yet the validation of this hypothesis prevails in the Raman and Infrared spectroscopy characterization.

Figure 2a, Table S1 shows the Raman spectra for the 6R-$CaSi_2$, an intense peak at 493 cm^{-1}, along with less intense ones at 127, 222, 283, 410 and 905 cm^{-1} can be observed. According to the literature, the first order Transversal Optical Phonon (TO) of a 2D silicon-based material appears at ~500 cm^{-1} (E2g Symmetry).[29] This mode is attributed to the Si-Si vibration in the planes, which in comparison with bulk Si (520 cm^{-1}) is shifted towards lower frequencies. The peaks at 127, 222, 283 and 410 cm^{-1} correspond to a combination of the Transverse Acoustic Phonon (TA) and Longitudinal Optical phonon (LO). The peak at 905 cm^{-1} indicates a second order Raman scattering involving two TO phonons.[29–34] Similarly, the Raman signature of the Siloxene (**Figure 2b, Table S1**) shows a main band at 497 cm^{-1}, accompanied by peaks at 288, 373, 636, 727, 903 and 2115 cm^{-1}. In analogy with $CaSi_2$, the Raman modes at 497, 288 and 903 cm^{-1} are assigned to the E2g vibration, the 2TA and the 2TO of the Si-Si in the Si layers, respectively. The mode at 497 cm^{-1} is accompanied by a shoulder, attributed

to the presence of residual c-Si. The bands at 635, 735 and 2115 cm^{-1} correspond to the appearance of Si-H vibrations after Ca deintercalation. [17,29,35,36]
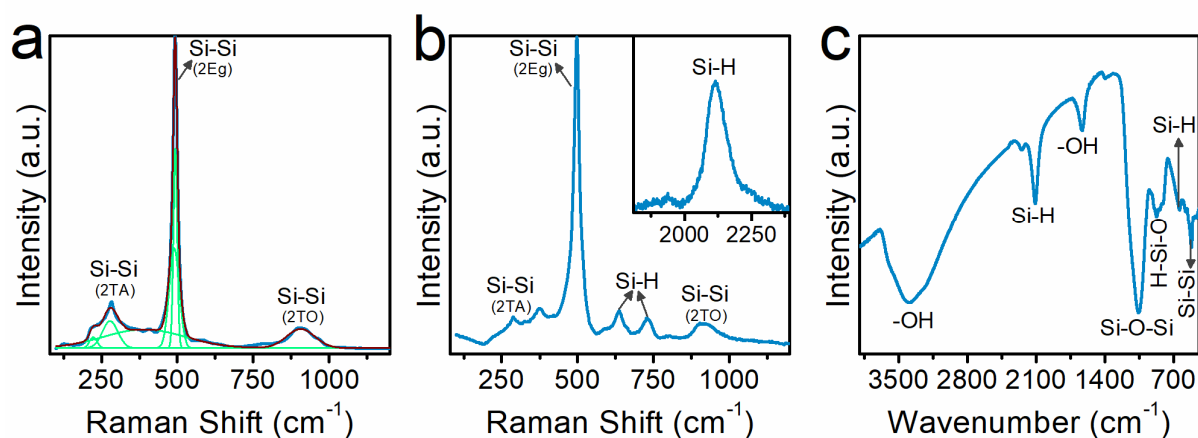

Figure 2. a) Deconvolution Raman spectra CaSi$_2$. **b)** raman spectra of Siloxene, **c)** Infrared spectra of Siloxene

Complementary information can be obtained by Infrared spectroscopy (**Figure 2c**), where several vibration bands can be distinguished (**Table S2**) at 465, 518, 643, 809, 875, 895, 1600, 2110 and 2250 cm^{-1}, with the most intense bands at 1060 and 3400 cm^{-1}. The peak at 518 cm^{-1} is assigned to the Si-Si mode in Si plane; that becomes active due to a dipole moment induced by the difference in electronegativity of the Si ligands (H and OH).[29] The Si-H vibrations can be found at 643 and 2110 cm^{-1}, the Si-OH, H-Si-O and H-SiO$_3$ at 875, 895 and 2250 cm^{-1}, respectively.[29,37,38] The –OH bending mode is characterized by a narrow line at 1628 cm^{-1} while the –OH groups that participate in a hydrogen bond are defined by a broad band at 3400 cm^{-1}.[27] The peak at 465 cm^{-1} corresponds to the Si-O-Si bending accompanied by the Si-O-Si symmetric and asymmetric stretching at 809 and 1060 cm^{-1}, respectively.[29] The appearance of the Si-O-Si modes in our siloxene indicates the presence of SiO$_x$ amorphous phases or an oxygen crosslinking (oxidation) between the planes. This oxidation occurs gradually and without any change in the stoichiometry as the oxygen from the –OH is

incorporated in the Si-planes in the form of Si-O-Si bridges, forming isolated Si_6 rings (Kautsky siloxene).

In summary, these findings indicate that indeed the Si planes from $CaSi_2$ are preserved in siloxene after Ca removal. The structure is predominantly constituted of Si rings terminated by OH and H, with a certain degree of Si-O-Si crosslinking.

3.2. Siloxene for metal (Li, Na, K)-ion batteries.

We have evaluated the potential use of siloxene as anode material for lithium, sodium and potassium ion batteries, the galvanostatic profiles are shown in **Figure 3**. The discharge capacities for the first cycle were 3958, 760 and 592 mAh/g for Li, Na and K, respectively. Unfortunately, a substantial amount of this capacity is irreversible and the second discharge delivered capacities of 2300, 311 and 203 mAh/g for Li, Na and K, respectively. Note that the conductive additive contributes with a reversible capacity of ~270 mAh/g for Li, ~120 mAh/g for Na and ~97 mAh/g for K (**Figures S4, S5**); though this approximation is not ideal and the real capacity could be lower for the composite electrode.

For the three systems the galvanostatic curves can be divided into three regions; i) a pseudo-plateau at 1.2V (only observed for the first discharge), ii) a sloping profile from 0.7-0.5V and iii) a steady decrease in the potential for voltages <0.5V. Likewise, the processes during charge can be categorized into a rapid increment of the potential until 0.3V, followed by a region with a gentle slope, after which either the potential increases gradually, as for Na, or abruptly, as for Li and K, until the end of charge. However, some differences are identified; for Li, in the second discharge a plateau at 0.5 V appears and prevails during the following cycles and for Na the plateau at 1.2V during the first discharge is enlarged compared to Li and K. The differential curves (**Figure 3**) supply complementary information; in the first cycle, for Li is possible to observe three peaks during reduction at 0.37, 0.16 and 0.06 V and during oxidation three peaks at 0.03, 0.3 and 0.45 V followed by a very broad signal. The second cycle (**Figure S6a**) resembles the first one, although the reduction peak at 0.37 V and the

8

oxidation one at 0.03 V are absent and a new reduction peak appears at 0.45 V, in line with the plateau observed in the galvanostatic curve. For Na, the reduction presents peaks at 1.10 and 0.09 V, and a very sharp one at 0.03 V, whereas the oxidation at 0.1 V and a broad signal at 0.6 V. In the second cycle (**Figure S6b**), no drastic change in the potential can be observed until 0.2 V, where, three peaks appear at 0.1, 0.06 and 0.02 V. The oxidation displays a peak at 0.01 V followed by a hump with a maximum at 0.6 V. For K, upon reduction two peaks appear at 0.13 and 0.04 V, while during oxidation a sharp peak is observed at 0.021 V and a well-defined one at 0.46 V. During the second cycle (**Figure S6c**), for reduction no significant variation can be observed, except for a very broad signal at approximately 0 V, while for oxidation two peaks take place at 0.021 and 0.46 V. These preliminary tests for potassium demonstrate the possible reversibility of K in the siloxene electrode; nevertheless, its electrochemical behavior and cyclability is dependent on several factors; particularly the electrolyte formulation.[39] The research for the optimal combination is ongoing and further details will be published elsewhere.

In analogy with the reports for the lithiation/sodiation of Silicon-based materials, the first discharge is characterized by a substantial amount of irreversible capacity, due to the formation of the Solid Electrolyte Interphase (SEI) layer, which can be enhanced by the–OH and –H groups present in the Siloxene surface. The plateau at 1.2 V could correspond as well to the reduction of the FEC additive. As evidenced, when no FEC is used, this plateau is absent and the cells delivered poor lithiation/sodiation capacities, confirming the importance of FEC in the overall performance.

The reported features for the sodiation of Si do not correspond to our results, except for the signature of Na insertion into the carbon additive. According to the literature, the galvanostatic curve for the sodiation of Si presents a sloping voltage region with a plateau at 0.5 and 0.1 V; the desodiation proceeds with a gradual increase in the voltage until the end of charge. Both processes are visualized in the derivative curve by two reduction peaks at 0.5

9

and 0.04 V and an oxidation one at 0.08 V. [40–42] The galvanostatic curve of the conductive carbon presents a sloping voltage region at >0.1 V (Na intercalation in the graphene layers) and a plateau at 0.05 V (Na intercalation into the pores), corresponding to a reduction peak at 0.8 and 0.020 V and an oxidation one at 0.1V[40,43]. In contrast, the lithiation of siloxene-based materials has been reported in the literature, and the electrochemistry seems to be closely related to the composition.[14,16,18,19]
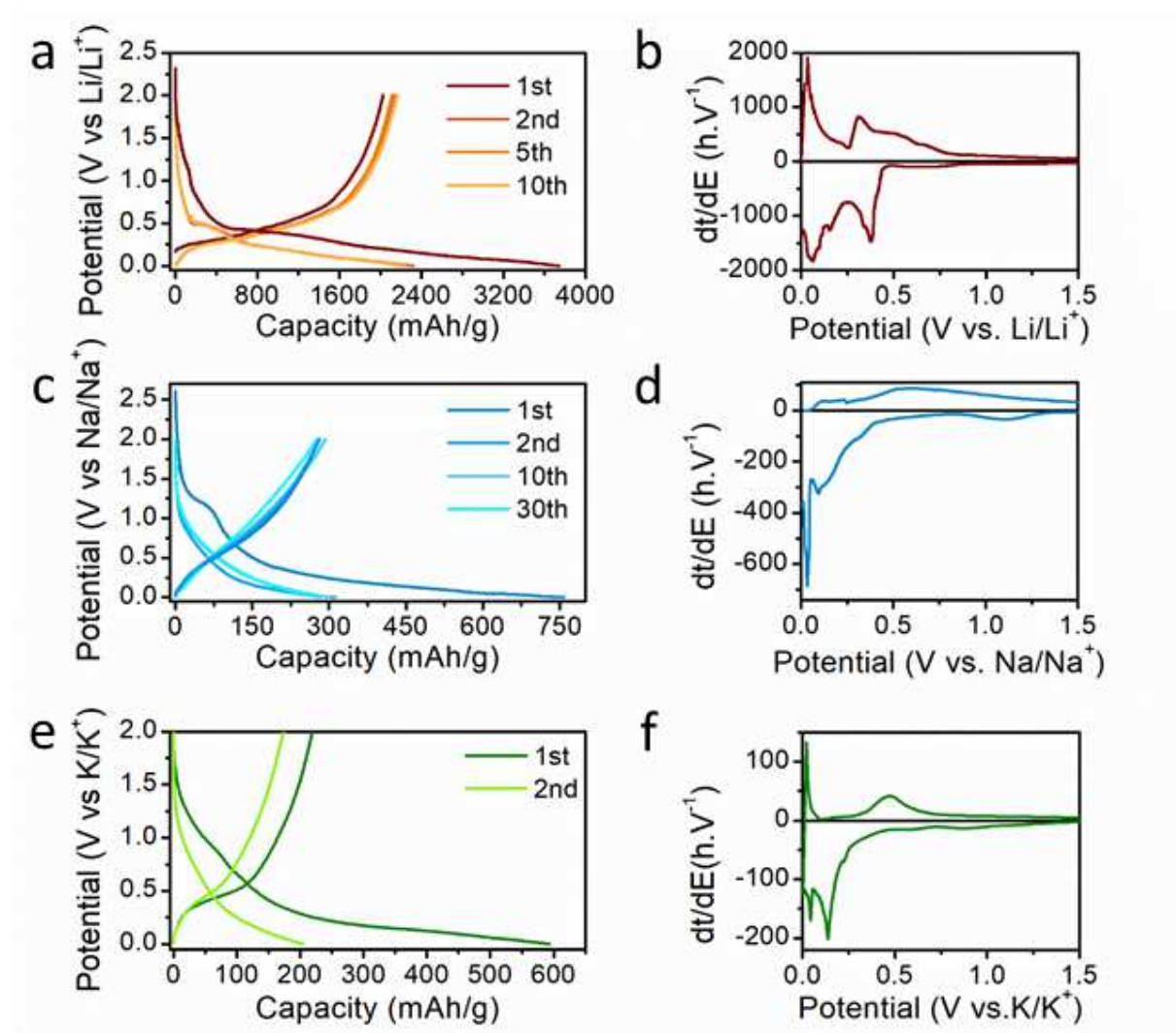

Figure 3. Galvanostatic curves and their respective derivative curves for the first cycle for siloxene vs **a, b)** Li, **c,d)** Na and **e,f)** K

In analogy with Na, the cycling vs Li presents almost no features corresponding to the alloying reaction with Si. In asmuch as no pseudo-plateau at 0.3 and 0.18 V during discharge appears, corresponding to the amorphization of c-Si and the crystallization of $Li_{15}Si_4$;

10

displayed in the derivative curve by two reduction peaks at 0.17 and 0.005 V and one at 0.45 V for oxidation. [44–49] In this sense, the peaks in the Siloxene derivative curve can be only partially attributed to this reaction due to the traces of c-Si, yet its signature is not reflected in the galvanostatic curve. Thus the observed phenomena might be originated from the insertion of Li in the carbon additive and the siloxene rather than an alloying Si/Li mechanism. Indeed the lithiation of siloxene can be evidenced by a prolonged sloping profile that extends until the end of the discharge in the galvanostatic curve. [14–19] In the derivative curve, the reduction peaks at 0.37, 0.16 and 0.006 V and the oxidation ones at 0.3 and 0.45 V are in line with the reports from Fu *et al*[17], Sun *et al*[16] and Zhang *et al*[18].

Finally, the capacity retention properties of siloxene were tested (**Figure 4 a, c**). Despite the irreversible character during the first cycle, the subsequent ones maintain significant reversible capacity values. Note that all the following values refer to the second cycle. For lithium, 1845 mAh/g are delivered after 58 cycles, representing a capacity retention of 79%. The coulombic efficiency increases from 51% to 91%, from the first to the second cycle and holds an average value of 96%. For sodium, 252 mAh/g are obtained after 77 cycles, corresponding to a capacity retention of 81%. The coulombic efficiency rapidly increases from 37% to 90% during the second cycle, and keeps an average value of 98% for the following ones. The improved capacity retention and high coulombic efficiency for Li compared to a pure Si electrode, is believed to be related with the lamellar character of siloxene; which buffers the volumetric changes during lithiation and shortens the Li diffusion distances.[44–49] Regarding the rate capability, the siloxene exhibits a good performance for both Li and Na. In **Figure 4 b,d** it is possible to observe that for rates of C/20 and C/10 there is not a dramatic decrease in the capacity. However, for Na at 1C, 2C and 5C the electrode delivered poor capacities. This drop might be originated from kinetic limitations given the higher Na radius size. For Li, even at high rates (1C, 2C, 5C) the electrode delivers considerable capacities values, superior than conventional graphite-based anodes. In both

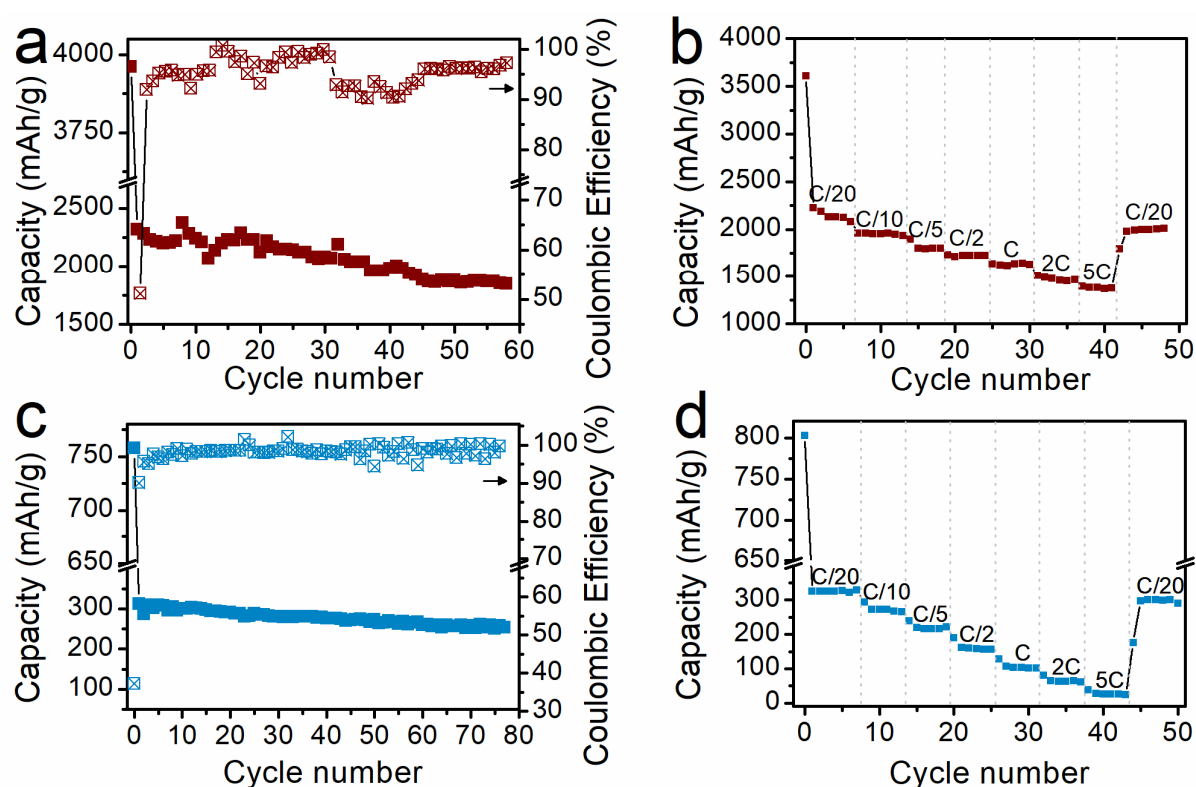cases, once the C/rate is reestablished to C/20 similar capacity values to the initial ones are recovered.

Figure 4. Cycling performance of siloxene vs **a)** Li and **c)** Na at C/20. Rate performance at different C/rates for siloxene vs **b)**Li and **d)** Na

3.2.1. Electrolyte solvent influence on the electrochemical cycling of Siloxene

The electrochemistry of silicon-based materials highly depends on factors like the intricate growth and poor stability of the SEI layer, the electrolyte and the nature of the electrode materials. In order to find favorable conditions for the cycling of siloxene alternative solvent mixtures to EC/DMC were tested: EC/DEC, EC/PC and Tetraglyme. Note that the XPF_6 (X=Na, Li) salt and the ratio of 1% FEC additive were kept constant. In this section we present an overview of the study; for additional details please refer to the **Supplementary Information** section.

For Na, (**Figure S7a,c,e**) the use of different solvents still delivers a substantial irreversible capacity during the first cycle; 750, 815, 880 and 950 mAh/g for EC/DMC, EC/DEC, EC/PC and tetraglyme, respectively. Correspondingly, the second cycle displayed capacities of 311,

12

350, 320 and 300 mAh/g. No significant changes were found in the galvanostatic curve profile, with the exception of tetraglyme, where the plateau at 1.2 V is enlarged, indicating probably a different reactivity with ether-based electrolytes. For Li, (**Figure S7b,d,f**) the capacities for the first discharge are 3958, 3577, 3319 and 3409 mAh/g for EC/DMC; EC/DEC, EC/PC and Tetraglyme, respectively, substantial amount of this capacity is irreversible and for the second discharge, the capacities are 2300, 2165, 2002 and 2302 mAh/g, respectively. Regarding the capacity retention (**Figure S8**), for Na, after 50 cyles EC/DEC retains 79%, EC/PC 84% tetraglyme 58% of the capacity with respect to the values observed during the second cycle.

In both cases, the EC/DMC and EC/DEC mixtures presented improved results, whereas for tetraglyme, despite the high capacities during the first cycles, it inevitably experienced rapid capacity fading. The high ionic conductivity and mobility in EC and the high viscosity and low conductivity in tetraglyme might be behind these two different behaviors. In addition, carbonate and ether-based electrolytes could have different reactivities with the siloxene surface, ratifying that the choice of solvent mixture is important to ensure an optimal cycling.

3.3. Electrochemical Mechanism insight

The electrochemical cycling of Siloxene suggests that an alternative mechanism to conventional alloying takes place. As previously presented the results show almost no evidence of the characteristic features for an alloying of Li/Na with Si. In this regard the intercalation of alkali into the siloxene layers is plausible and desired to avoid the volume change during the discharge/charge cycles. In order to understand the possible electrochemical mechanism taking place, the discharged and charged material was characterized by Raman and IR spectroscopy, complimented with microscopy techniques.

3.3.1. Characterization of discharged and charged compound.

13

Figure 5 a,b shows the Raman spectra for the CaSi$_2$, siloxene and discharged and charged product for Na and Li, the same basic structure of Si-Si in Si-planes defined by an intense peak centered between 492-507 cm^{-1} and the second order TA and TO at 283 and 900 cm^{-1}, can be observed in all of them. Note that upon Ca deintercalation from CaSi$_2$ to form siloxene, new bands at 635, 735 and 2115 cm^{-1} appear, ascribed to the Si-H vibrations. These bands disappear upon electrochemical (de)sodiation/(de)lithiation but the Si planes vibration modes are preserved, indicating no structural degradation with cycling. Additional bands emerge at 1330 and 1600 cm^{-1}, corresponding to the disordered (D) A$_{1g}$ breathing mode of defects/vibrations and the graphitized (G) E$_{2g}$ vibration of the C-C plane from the conductive carbon.[50] Interestingly, the main Si planes Raman band position seems to be related with the composition, that is, for CaSi$_2$ it is centered at 493 cm^{-1} and at 497 cm^{-1} once the Ca is replaced by –H and –OH in siloxene. Upon sodiation/lithiation it shifts to 504 and 505 cm^{-1}; and after desodiation/delithiation to 494 and 492 cm^{-1}, respectively. We believe that this shift is probably related with a change in the interlayer separation and in the bond nature between the Si-planes and the substituent group, meaning that upon electrochemical (de)sodiation/(de)lithiation the –H and –OH bonds in siloxene are probably replaced by the alkali ion, resulting in a reversible Raman shift.

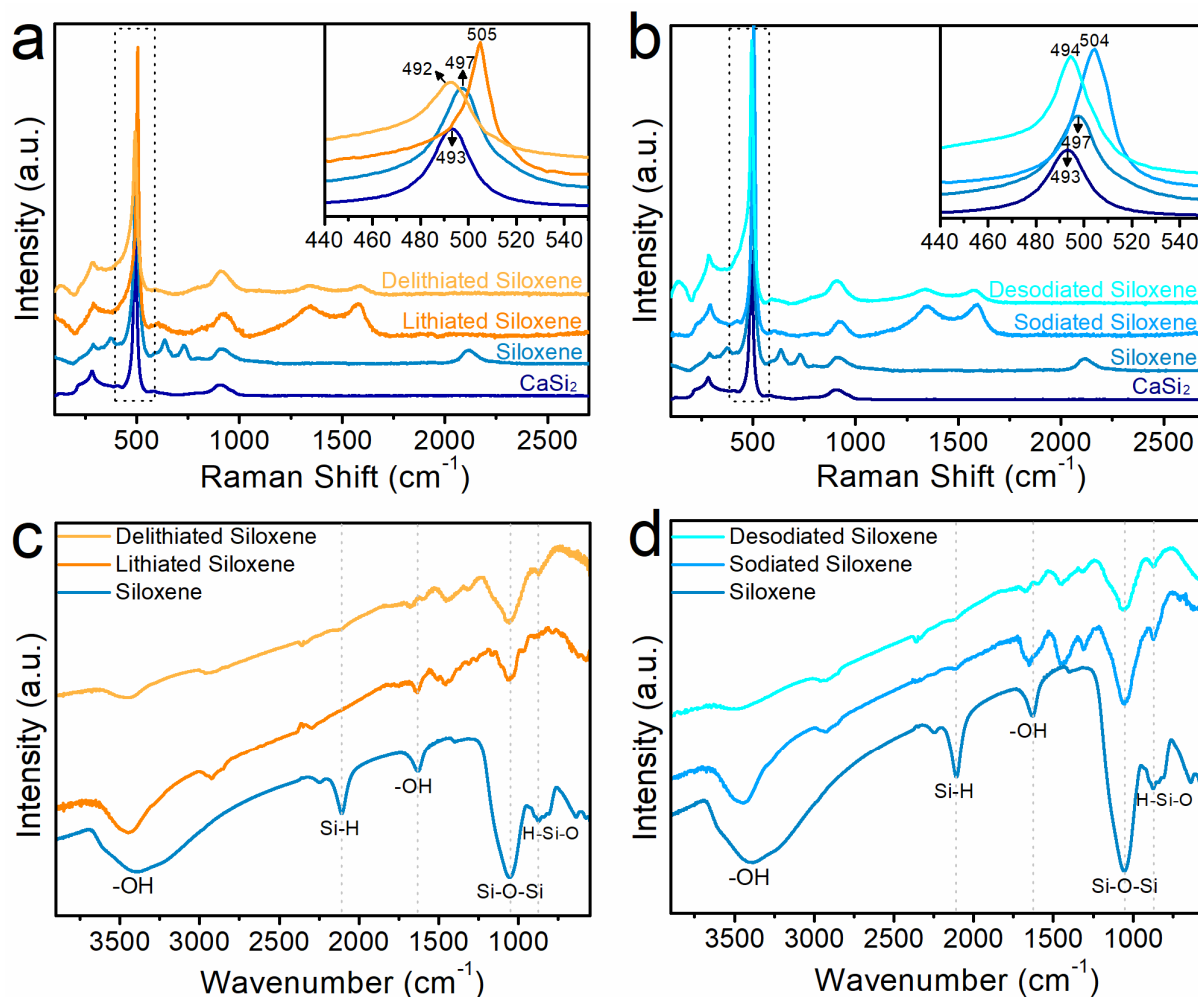**Figure 5. a)** Raman spectra of **a)** $CaSi_2$, siloxene and lithiated/delithiated siloxene and **b)** $CaSi_2$, siloxene and sodiated/desodiated siloxene. **c)** IR spectra of **a)** siloxene and lithiated/delithiated siloxene and **d)** siloxene and sodiated/desodiated siloxene

The IR spectra for the cycled electrodes are shown in **Figure 5 c,d;** for both Li and Na the Si-O-Si, H-Si-O bands are preserved while the –OH ones have decreased in intensity for the sodiated/lithiated sample and almost disappeared for the desodiated/delithiated one. Additional bands appear at 1445 and 1310 cm^{-1}, probably originated from carbonate-based products from the electrolyte decomposition deposited on the electrode surface, reports in literature locate these vibrations at 1650 (C=O), 1398 (C–H), 1300 (C=O) cm^{-1}.[50] In agreement with the Raman spectroscopy observations, the Si-H bands have almost disappeared for the cycled electrodes, suggesting a change in the bond nature, probably due to a new interaction with Na/Li ions, while the preservation of the H-Si-O and Si-O-Si bands

15

could indicate the stability of the Si planes with no degradation into silicates upon reaction with the alkali.
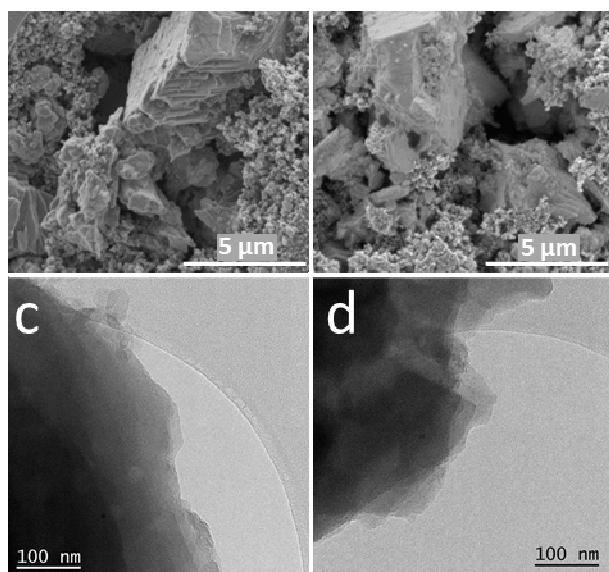

Figure 6. SEM picture for the **a)** lithiated and **b)** sodiated siloxene. **c, d)** TEM picture of sodiated siloxene

In order to examine the layered structure stability after prolonged cycling, the same analysis was performed after 100 cycles (**Figure S9**). The Raman signature of the Si-planes is still present, with the main band centered at 486 cm^{-1} for Na and 508 cm^{-1} for Li. This difference in shift could be related with the depth of sodiation/lithiation at the time of the analysis. In the IR spectra, for both cases, the –OH bands have practically disappeared, and the –OH bending at 1628 cm^{-1} has been replaced by two new bands situated at approximately the same frequency. The bands at 1450 and 1300 cm^{-1} and Si-O-Si signal are preserved.

Lastly to complement the Raman and IR findings, the cycled electrodes were analyzed by SEM and TEM (**Figure 6, S10**). After the first discharge-charge and even after 100 cycles, the lamellar compound was still present (in line with the Si-planes structure stability). Notably, the aggregate size has decreased after 100 cycles. The TEM analysis of the sodiated siloxene confirms the conservation of the lamellar character (**Figure 6, S11**), although the material remains amorphous as shown by the electron diffraction. The EDX analysis (**Table S3**) indicates the presence of silicon (44%), oxygen (38.55%) and Sodium (14.34%) as the main

components with minor traces of Cl, Ca, P and F as residues from the synthesis process and the electrolyte.

The combined Raman and IR spectroscopy complemented with SEM and TEM provide information on the electrochemical mechanism of sodiation/lithiation of siloxene. The results demonstrate the stability of the siloxene Si-plane structure upon cycling and the reversible insertion of Na/Li into the carbon additive, as already predicted in the standard coin cell cycling (**Figure S4,S5**). Nonetheless, the carbon additive cannot explain the totality of the delivered capacities, meaning that siloxene undergoes an electrochemical reaction with Na and Li. Generally, silicon-based materials are most known to undergo an alloying reaction with Li and Na, however in the present study neither the galvanostatic nor the derivative curves of siloxene exhibit the characteristic features of such process. Besides, an XRD analysis (**Figure S12**) of the siloxene at different potentials did not show any of the diffraction peaks from $NaSi/Li_{15}Si_4$ (both crystalline) at the end of the discharge, proper from the alloying mechanism. The NaSi[51] and some of the Li_xSi[52] phases are Raman active, yet, our Raman experiments did not show any of their vibration bands (**Figure S13**). The possibility of an alloy mechanism lies then in the presence of bulk Si as an impurity, even though its Raman signature is approximately in the same range as siloxene, only a particle size of 1-2 nm would provide an extremely broad band at ~500 cm^{-1} [33,53], thus this approach fails to explain our findings. In fact, the Raman shift in siloxene with respect bulk Si has its origins in the breaking of the translational symmetry in one direction (perpendicular to the plane) due to the 2D structure. Additionally, the modes at 172 and 210 cm^{-1} in siloxene are not present for bulk Si.[54]

The absence of these features from an alloying mechanism sets a pathway for an alternative interpretation, such the intercalation of Na and Li in the siloxene layers. Essential indicators from this reaction are the preservation of the lamellar character even after 100 cycles, the presence of Na in the discharged compound as observed by EDX, the reversible Raman shift

17

of the main Si-plane band for the discharged and charged electrode and the loss of the –OH and Si-H vibrations in Raman and IR spectroscopy. Undoubtedly, these two last ones are likely related to a change in the bond nature of the Si-planes with the substituent group producing a different interlayer separation, probably the electrochemical cycling induces an exchange between –OH and –H with Li/Na. Indeed, the theory predicts that the alkali ions adsorption leads to a geometrical transformation in order to accommodate more ions in alternative sites to the Si honeycomb hollow (most favored).[9] The intercalation of Na/Li into a layered Si-based materials has only been theoretically predicted for a single layer of siloxene (silicene), with no experimental record. The calculations foresee a high coverage of the silicene with alkali ions like Na, Li and K due to the nature of their interactions. The full sodiated/lithiated state of silicene corresponds to X_1Si_1 (X=Li/Na), the predicted binding energies and diffusion barriers indicate that their intercalation is achievable without the kinetic limitations (higher diffusion coefficient for silicene), structure degradation and volume expansion of bulk Si. [9,11,55–57] This feasibility for alkali intercalation with such high structural stability introduces siloxene as a potential anode for LIB, NIB and KIB batteries. Nevertheless, a better understanding of its electrochemical mechanism is necessary to develop its maximum performance.

4. Conclusion

In conclusion, the siloxene was obtained from topotactic deintercalation of Ca from $CaSi_2$, and the obtained structure consisted of Si honeycombs planes, saturated with –H and –OH. The siloxene has exhibited potential application as anode material for LIB, NIB and KIB technologies, and despite the high irreversible capacity delivered during the first discharge, reversible capacities of 2300, 311 and 203 mAh/g were delivered for Li, Na and K, respectively. The electrode material performed with excellent capacity retention and coulombic efficiency for LIB and NIB. Additionally, an intercalation mechanism for the

18

siloxene cycling was proposed based on the experimental findings by Raman and IR spectroscopy complemented by SEM and TEM. It is worth noting that it is the first time that a Silicon-based electrode material shows such high stable capacity without volume expansion and its associated consequences on the performance, representing a real breakthrough for the batteries field. Nevertheless, further experiments must be carried out for an advanced understanding, particularly the role of the different surface groups during the first discharge and the determination of the optimal cycling conditions for an improved performance. Finally, the family of the lamellar Zintl phases has demonstrated a vast versatility for different applications, opening their study as new anode materials for different battery technologies.

Supporting Information

Supporting Information is available. Additional details on the characterization of $CaSi_2$ and Siloxene. Electrochemical cycling of the carbon conductive additive. Derivative curves for the second cycle of siloxene vs Li, Na and K. Electrolyte influence on the siloxene cycling. Raman and infrared spectra for the siloxene electrode after 100 cycles. SEM and TEM pictures for the cycled siloxene electrodes. In situ XRD of the cycling of a siloxene electrove vs Li. Raman spectra of different lithiated references. Tables with additional details from the Raman, infrared and EDX characterization.
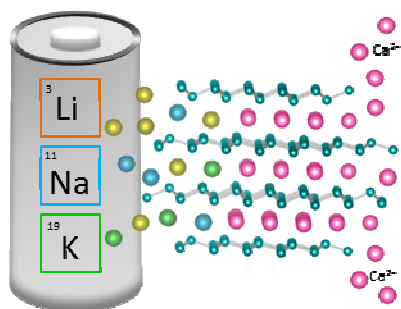
References

[1]   M.T. McDowell, S.W. Lee, W.D. Nix, Y. Cui, 25th anniversary article: Understanding the lithiation of silicon and other alloying anodes for lithium-ion batteries, Adv. Mater. 25 (2013) 4966–4985. doi:10.1002/adma.201301795.

[2]   C.Y. Chou, M. Lee, G.S. Hwang, A Comparative First-Principles Study on Sodiation of Silicon, Germanium, and Tin for Sodium-Ion Batteries, J. Phys. Chem. C. (2015). doi:10.1021/acs.jpcc.5b01099.

[3]   U. Dettlaff-Weglikowska, W. Hönle, A. Molassioti-Dohms, S. Finkbeiner, J. Weber, Structure and optical properties of the planar silicon compounds polysilane and Wohler siloxene, Phys. Rev. B. 56 (1997) 13132–13140. doi:DOI 10.1103/PhysRevB.56.13132.

[4]   A. Weiss, G. Beil, H. Meyer, The Topochemical Reaction of CaSi2 to a Two-Dimensional Subsiliceous Acid Si6H3(OH)3 (= Kautskys' Siloxene), Zeitschrift Fur Naturforsch. 34b (1979) 25–30. doi:10.1515/znb-1980-0108.

[5]   F. Wöhler, Ueber Verbindungen des Siliciums mit Sauerstoff und Wasserstoff, Justus Liebigs Ann. Chem. 127 (1863) 257–274. doi:10.1002/jlac.18631270302.

[6]   H. Kautsky, Über einige ungesättigte Siliciumverbindungen, Zeitschrift Für Anorg. Und Allg. Chemie. 117 (1921) 209–242. doi:10.1002/zaac.19211170115.

[7]   M.A. Ali, M.R. Tchalala, Chemical Synthesis of Silicon Nanosheets from layered calcium disilicide, J. Phys. Conf. Ser. 491 (2014) 12009. doi:10.1088/1742-6596/491/1/012009.

[8]   M. Houssa, A. Dimoulas, A. Molle, Silicene: A review of recent experimental and theoretical investigations, J. Phys. Condens. Matter. 27 (2015) 253002. doi:10.1088/0953-8984/27/25/253002.

[9]   J. Zhuang, X. Xu, G. Peleckis, W. Hao, S.X. Dou, Y. Du, Silicene: A Promising Anode for Lithium-Ion Batteries, Adv. Mater. (2017) 1606716. doi:10.1002/adma.201606716.

[10]   G.A. Tritsaris, E. Kaxiras, S. Meng, E. Wang, Adsorption and diffusion of lithium on layered silicon for Li-ion storage, Nano Lett. 13 (2013) 2258–2263. doi:10.1021/nl400830u.

[11]   V. V Kulish, O.I. Malyi, M.-F. Ng, Z. Chen, S. Manzhos, P. Wu, Controlling Na diffusion by rational design of Si-based layered architectures., Phys. Chem. Chem. Phys. 16 (2014) 4260–7. doi:10.1039/c3cp54320j.

[12]   J. Zhao, H. Liu, Z. Yu, R. Quhe, S. Zhou, Y. Wang, C.C. Liu, H. Zhong, N. Han, J. Lu, Y. Yao, K. Wu, Rise of silicene: A competitive 2D material, Prog. Mater. Sci. 83 (2016) 24–151. doi:10.1016/j.pmatsci.2016.04.001.

[13]   J. Zhu, U. Schwingenschlögl, Silicene for Na-ion battery applications, 2D Mater. 3 (2016) 35012. doi:10.1088/2053-1583/3/3/035012.

[14]   Y. Kumai, H. Nakano, Characteristics of layered polysilane and its application to lithium ion battery anodes, Jpn. J. Appl. Phys. (2015) 35201. doi:10.7567/JJAP.54.035201.

[15]   K. Xu, L. Ben, H. Li, X. Huang, Silicon-based nanosheets synthesized by a topochemical reaction for use as anodes for lithium ion batteries, Nano Res. 8 (2015) 2654–2662. doi:10.1007/s12274-015-0772-4.

[16]   L. Sun, T. Su, L. Xu, M. Lui, H.-B. Du, Two-dimensional ultra-thin SiO x (0 < x < 2) nanosheets with long-term cycling stability as lithium ion battery anodes, Chem. Commun. 52 (2016) 4341–4344. doi:10.1039/C6CC00723F.

[17]   R. Fu, K. Zhang, R. Proietti, H. Huang, Y. Xia, Two-dimensional silicon suboxides nanostructures with Si nanodomains confined in amorphous SiO2 derived from siloxene as high performance anode for Li-ion batteries, Nano Energy. 39 (2017) 546–553. doi:10.1016/j.nanoen.2017.07.040.

[18]   X. Zhang, X. Qiu, D. Kong, L. Zhou, Z. Li, X. Li, L. Zhi, Silicene Flowers: A Dual

Stabilized Silicon Building Block for High-Performance Lithium Battery Anodes, ACS Nano. 11 (2017) 7476–7484. doi:10.1021/acsnano.7b03942.

[19] H. Imagawa, H. Itahara, Stabilized lithium-ion battery anode performance by calcium-bridging of two dimensional siloxene layers, Dalt. Trans. 46 (2017) 3655–3660. doi:10.1039/C6DT03837A.

[20] H. Nakano, T. Mitsuoka, M. Harada, K. Horibuchi, H. Nozaki, N. Takahashi, T. Nonaka, Y. Seno, H. Nakamura, Soft synthesis of single-crystal silicon monolayer sheets, Angew. Chemie - Int. Ed. 45 (2006) 6303–6306. doi:10.1002/anie.200600321.

[21] M.Q. Arguilla, N.D. Cultrara, M.R. Scudder, S. Jiang, R.D. Ross, J.E. Goldberger, Optical properties and Raman-active phonon modes of two-dimensional honeycomb Zintl phases, J. Mater. Chem. C. 5 (2017) 11259–11266. doi:10.1039/C7TC01907F.

[22] P. Bordet, M. Affronte, S. Sanfilippo, M. Nunez-Regueiro, O. Laborde, G.L. Olcese, A. Palenzona, S. LeFloch, D. Levy, M. Hanfland, Structural phase transitions in CaSi 2 under high pressure, Phys. Rev. B. 62 (2000) 392–397. doi:10.1103/PhysRevB.62.11392.

[23] V.A. Drits, C. Tchoubar, X-Ray Diffraction by Disordered Lamellar Structures, Springer-Verlag Berlin Heidelberg, 1990. doi:10.1007/978-3-642-74802-8.

[24] G.U. Vogg, M.S. Brandt, M. Stutzmann, M. Albrecht, From CaSi2 to siloxene: Epitaxial silicide and sheet polymer films on silicon, J. Cryst. Growth. 203 (1999) 570–581. doi:10.1016/S0022-0248(99)00135-9.

[25] J.R. Dahn, B.M. Way, E. Fuller, Structure of Siloxene and Layered Polysilane (Si6H6), Phys. Rev. B. 48 (1993) 872–877. doi:10.1103/PhysRevB.48.17872.

[26] H. Stüger, Kautsky-siloxene analogous monomers and oligomers, in: P. Jutzi, U. Schubert (Eds.), Silicon Chem. From Atom to Ext. Syst., Wiley-VCH Verlag GmbH & Co, 2007: pp. 214–225. doi:10.1002/9783527610761.ch16.

[27] M.S. Brandt, G. Vogg, M. Stutzmann, Silicon- and germanium-based sheet polymers and zintl phases, in: P. Jutzi, U. Schubert (Eds.), Silicon Chem. From Atom to Ext. Syst., Wiley-VCH Verlag GmbH & Co, 2007: pp. 194–213. doi:10.1002/9783527610761.ch15.

[28] M. Stutzmann, M.S. Brandt, M. Rosenbauer, H.D. Fuchs, S. Finkbeiner, J. Weber, P. Deak, Luminescence and optical properties of siloxene, J. Lumin. 57 (1993) 321–330. doi:10.1016/0022-2313(93)90150-L.

[29] H.D. Fuchs, M. Stutzmann, M.S. Brandt, M. Rosenbauer, J. Weber, A. Breitschwerdt, P. Deak, M. Cardona, Porous silicon and siloxane- vibrational and structural properties, Phys. Rev. B. 48 (1993) 8172–8189. doi:10.1103/PhysRevB.48.8172.

[30] S.-L. Zhang, Theoretical Fundamentals of Raman Scattering in Solids, in: S.-L. Zhang (Ed.), Raman Spectrosc. Its Appl. Nanostructures, John Wiley & Sons, Ltd, 2012: pp. 199–247. doi:10.1002/9781119961659.ch7.

[31] X. Yu, F. Xue, H. Huang, C. Liu, J. Yu, Y. Sun, X. Dong, G. Cao, Y. Jung, Synthesis and electrochemical properties of silicon nanosheets by DC arc discharge for lithium-ion batteries, Nanoscale. 6 (2014) 6860–6865. doi:10.1039/C3NR06418B.

[32] R. Wang, G. Zhou, Y. Liu, S. Pan, H. Zhang, D. Yu, Z. Zhang, Raman spectral study of silicon nanowires: High-order scattering and phonon confinement effects, Phys. Rev. B. 61 (2000) 16827–16832. doi:10.1103/PhysRevB.61.16827.

[33] G. Faraci, S. Gibilisco, A.R. Pennisi, C. Faraci, Quantum size effects in Raman spectra of Si nanocrystals, J. Appl. Phys. 109 (2011) 074311 1-4. doi:10.1063/1.3567908.

[34] J. Yu, J. Gao, F. Xue, X. Yu, H. Yu, X. Dong, H. Huang, A. Ding, X. Quan, G. Cao, Formation mechanism and optical characterization of polymorphic silicon nanostructures by DC arc-discharge, RSC Adv. 5 (2015) 68714–68721. doi:10.1039/C5RA11738K.

[35] M.S. Brandt, L. Höppel, N. Zamanzadeh-Hanebuth, G. Vogg, M. Stutzmann,

Vibrational anti-crossing in siloxene, Phys. Status Solidi Basic Res. 215 (1999) 409–412. doi:10.1002/(SICI)1521-3951(199909)215:1<409::AID-PSSB409>3.0.CO;2-G.

[36] P. Vora, S.A. Solin, P. John, Raman scattering from pristine and oxidized polysilanes, Phys. Rev. B. 29 (1984) 3423–3429. doi:10.1103/PhysRevB.29.3423.

[37] H.D. Fuchs, M. Stutzmann, M.S. Brandt, M. Rosenbauer, J. Weber, M. Cardona, Visible luminescence from porous silicon and siloxene, Phys. Scr. T45 (1992) 309–313. doi:10.1088/0031-8949/1992/T45/067.

[38] S. Yamanaka, H. Matsu-ura, M. Ishikawa, New deintercalation reaction of calcium from calcium disilicide. Synthesis of layered polysilane, Mater. Res. Bull. 31 (1996) 307–316. doi:10.1016/0025-5408(95)00195-6.

[39] L. Madec, V. Gabaudan, G. Gachot, L. Stievano, L. Monconduit, H. Martinez, Paving the Way for K-Ion Batteries: Role of Electrolyte Reactivity through the Example of Sb-Based Electrodes, ACS Appl. Mater. Interfaces. (2018) acsami.8b08902. doi:10.1021/acsami.8b08902.

[40] Y. Xu, E. Swaans, S. Basak, H.W. Zandbergen, D.M. Borsa, F.M. Mulder, Reversible na-ion uptake in Si nanoparticles, Adv. Energy Mater. 6 (2016) 1–5. doi:10.1002/aenm.201501436.

[41] M. Shimizu, H. Usui, K. Fujiwara, K. Yamane, H. Sakaguchi, Electrochemical behavior of SiO as an anode material for Na-ion battery, J. Alloys Compd. 640 (2015) 440–443. doi:10.1016/j.jallcom.2015.03.171.

[42] L. Zhang, X. Hu, C. Chen, H. Guo, X. Liu, G. Xu, H. Zhong, S. Cheng, P. Wu, J. Meng, Y. Huang, S. Dou, H. Liu, In Operando Mechanism Analysis on Nanocrystalline Silicon Anode Material for Reversible and Ultrafast Sodium Storage, Adv. Mater. (2016). doi:10.1002/adma.201604708.

[43] B. Peng, Y. Xu, X. Wang, X. Shi, F.M. Mulder, The electrochemical performance of super P carbon black in reversible Li/Na ion uptake, Sci. China Physics, Mech. Astron. 60 (2017) 4–13. doi:10.1007/s11433-017-9022-y.

[44] M.N. Obrovac, L. Christensen, Structural Changes in Silicon Anodes during Lithium Insertion-Extraction, J. Electrochem. Soc. 7 (2004) A93–A96. doi:10.1149/1.1652421.

[45] F. Wang, L. Wu, B. Key, X. Yang, C.P. Grey, Y. Zhu, J. Graetz, Electrochemical Reaction of Lithium with Nanostructured Silicon Anodes : A Study by In-Situ Synchrotron X-Ray Diffraction and Electron Energy-Loss Spectroscopy, Adv. Energy Mater. 3 (2013) 1324–1331. doi:10.1002/aenm.201300394.

[46] D.S.M. Iaboni, M.N. Obrovac, Li15Si4 Formation in Silicon Thin Film Negative Electrodes, J. Electrochem. Soc. 163 (2016) 255–261. doi:10.1149/2.0551602jes.

[47] J.Y. Kwon, J. Heon, S.M. Oh, Performance of electrochemically generated Li21Si5 phase for lithium-ion batteries, Electrochim. Acta. 55 (2010) 8051–8055. doi:10.1016/j.electacta.2010.01.054.

[48] J. Li, J.R. Dahn, An In Situ X-Ray Diffraction Study of the Reaction of Li with Crystalline Si, J. Electrochem. Soc. 154 (2007) A156–A161. doi:10.1149/1.2409862.

[49] Y. Kang, S. Lee, S. Kim, G. Jeong, M. Sung, W. Choi, S. Kim, Phase transitions explanatory of the electrochemical degradation mechanism of Si based materials, Electrochem. Commun. 9 (2007) 959–964. doi:10.1016/j.elecom.2006.11.036.

[50] P. Lanz, P. Novak, Combined In Situ Raman and IR Microscopy at the Interface of a Single Graphite Particle with Ethylene Carbonate/Dimethyl Carbonate, J. Electrochem. Soc. 161 (2014) A1555–A1563. doi:10.1149/2.0021410jes.

[51] B.G. Kliche, M. Schwarz, Raman Spectrum of the Tetrasilatetrahedrane Anion Si4(4-), Angew. Chemie Int. Ed. English. 26 (1987) 349–351.

[52] T. Gruber, D. Thomas, C. Röder, J. Kortus, C. Röder, F. Mertens, J. Kortus, Raman spectroscopic studies of LixSiy compounds, J. Raman Spectrosc. 44 (2013) 934–938. doi:10.1002/jrs.4308.

[53] E. Cinquanta, E. Scalise, D. Chiappe, C. Grazianetti, B. Van Den Broek, M. Houssa, M. Fanciulli, A. Molle, Getting through the nature of silicene: An sp2-sp3 two-dimensional silicon nanosheet, J. Phys. Chem. C. 117 (2013) 16719–16724. doi:10.1021/jp405642g.

[54] P. De Padova, C. Ottaviani, C. Quaresima, B. Olivieri, P. Imperatori, E. Salomon, T. Angot, L. Quagliano, C. Romano, A. Vona, M. Muniz-Miranda, A. Generosi, B. Paci, G. Le Lay, 24H Stability of Thick Multilayer Silicene in Air, 2D Mater. 1 (2014). doi:10.1088/2053-1583/1/2/021003.

[55] X. Lin, J. Ni, Much stronger binding of metal adatoms to silicene than to graphene: A first-principles study, Phys. Rev. B - Condens. Matter Mater. Phys. 86 (2012) 1–9. doi:10.1103/PhysRevB.86.075440.

[56] H. Oughaddou, H. Enriquez, M.R. Tchalala, H. Yildirim, A.J. Mayne, A. Bendounan, G. Dujardin, M. Ait Ali, A. Kara, Silicene, a promising new 2D material, Prog. Surf. Sci. 90 (2015) 46–83. doi:10.1016/j.progsurf.2014.12.003.

[57] B. Mortazavi, A. Dianat, G. Cuniberti, T. Rabczuk, Application of silicene, germanene and stanene for Na or Li ion storage: A theoretical investigation, Electrochim. Acta. 213 (2016) 865–870. doi:10.1016/j.electacta.2016.08.027.

Graphical Abstract